Simulation of cold plasma in a chamber under high- and low-frequency voltage conditions for a capacitively coupled plasma*

Hao Daoxin(郝道欣), Cheng Jia(程嘉)†, Ji Linhong(季林红), and Sun Yuchun(孙钰淳)

Department of Precision Instruments and Mechanology, Tsinghua University, Beijing 100084, China

Abstract: The characteristics of cold plasma, especially for a dual-frequency capacitively coupled plasma (CCP), play an important role for plasma enhanced chemical vapor deposition, which stimulates further studies using different methods. In this paper, a 2D fluid model was constructed for N_2 gas plasma simulations with CFD-ACE+, a commercial multi-physical software package. First, the distributions of electric potential (E_{pot}), electron number density (N_e), N number density (N) and electron temperature (T_e) are described under the condition of high frequency (HF), 13.56 MHz, HF voltage, 300 V, and low-frequency (LF) voltage, 0 V, particularly in the sheath. Based on this, the influence of HF on N_e is further discussed under different HF voltages of 200 V, 300 V, 400 V, separately, along with the influence of LF, 0.3 MHz, and various LF voltages of 500 V, 600 V, 700 V. The results show that sheaths of about 3 mm are formed near the two electrodes, in which E_{pot} and T_e vary extensively with time and space, while in the plasma bulk E_{pot} changes synchronously with an electric potential of about 70 V and T_e varies only in a small range. N is also modulated by the radio frequency, but the relative change in N is small. N_e varies only in the sheath, while in the bulk it is steady at different time steps. So, by comparing N_e in the plasma bulk at the steady state, we can see that N_e will increase when HF voltage increases. Yet, N_e will slightly decrease with the increase of LF voltage. At the same time, the homogeneity will change in both x and y directions. So both HF and LF voltages should be carefully considered in order to obtain a high-density, homogeneous plasma.

Key words: plasma; CFD-ACE+; HF; LF; voltage; sheath

DOI: 10.1088/1674-4926/33/10/104004 **EEACC:** 2550

1. Introduction

In the manufacture of integrated circuits, as much as a third of the production process, such as etching, physical vapor deposition (PVD), and plasma enhanced chemical vapor deposition (PECVD), is related to the use of cold plasma. The trial-and-error method is widely used in the design of the plasma chamber due to the complex chemical reactions, highly nonlinear characteristics and the large span in time and space scales of the plasma. Single-frequency capacitively coupled plasmas (SF-CCPs) were first used in industry, but dual-frequency CCPs (DF-CCPs) attract more research groups' attention for their functional separation of plasma sustainability and ion bombardment. Braginsky *et al.*[1] discovered that when the total power is fixed, the efficiency and Ne of DF-CCPs are higher than those of traditional SF-CCPs. Pu's group[2−4] in Tsinghua University carried out extensive research on plasma detection and CCP discharge experiments.

Researchers have been trying to avoid the potentially large waste of time and energy, and to anticipate the effects of the plasma under different conditions through modeling and simulation. In order to fully and accurately describe the special characteristics of a plasma in a dual-frequency CCP reactor, many kinds of simulation methods have been developed, such as the particle-in-cell (PIC) model, fluid model or the hybrid model. Georgieva[5] studied the discharge process of DF-CCPs, using the PIC/MCC method. Alabas and Brinkmann[6] used the fluid model and discovered that the radio frequency (RF) resources will be coupled with each other when the two frequencies are similar, resulting in higher plasma density. Wang's research group[7−9] at Dalian University of Technology developed a DF-CCP discharge device and built hybrid models to carry out in-depth research on the decoupling of DF-CCPs, the sheath characteristics, the ion energy and angular distribution. They used a hybrid model for the simulation of the DF-CCP discharge, which is based on a fluid model for calculating the entire region and a Monte Carlo model in the sheath to simulate the ion energy distributions and the ion angle distributions[10]. Kushner and Economou developed a hybrid plasma equipment model (HPEM)[11] in 1994, and a hybrid model was used by Rakhimova[12] to discuss the discharge mode at high frequency (HF) and low frequency (LF), in which the PIC/MCC model was used only for electrons, and the fluid model was used for ion concentrations to speed up the calculation.

In this paper, a two-dimensional PECVD model was built with CFD-ACE+, a commercial multi-physical software package, which solves the plasma parameters under different voltages of dual-RFs in fluid mode. The high speed calculation and improved model make this method increasingly popular for researchers wishing to know about the characteristics of the plasma in advance. Later, the computational models and governing equations used in this simulation are described. The distribution of E_{pot}, N_e, N and T_e are discussed as well as the influence of HF and LF voltages to the plasma bulk.

* Project supported by the Important National Science & Technology Specific Projects No.2 (No. 2011ZX02403-004) and the Independent Research Subject from the State Key Laboratory of Tribology in Tsinghua University (No. SKLT11C2).

† Corresponding author. Email: chengjia@mail.tsinghua.edu.cn

Received 29 March 2012, revised manuscript received 7 June 2012

© 2012 Chinese Institute of Electronics

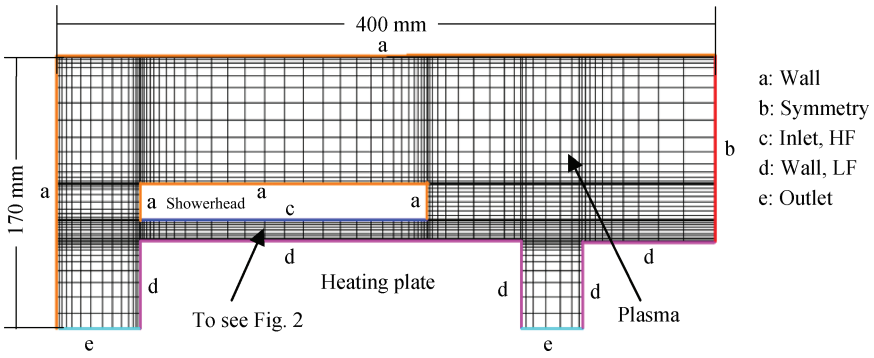

Fig. 1. 2D CCP model of the PECVD.

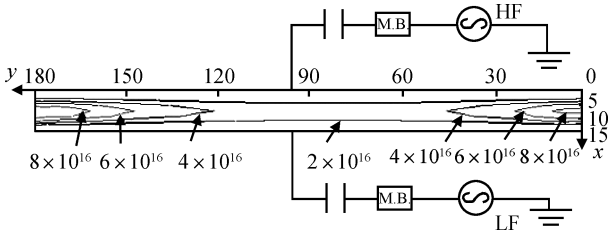

Fig. 2. Two electrodes of the CCP and the distribution of N_e (HF = 300 V@13.56 Hz, LF = 0 V).

2. Modeling and governing equations

The PECVD chamber can be considered as a revolving body, and its two-dimensional geometry and mesh model can be constructed from the rotating cross section of the cylinder plasma chamber, as shown in Fig. 1. The chamber radius is 400 mm, the inlet is 180 mm wide and the two outlets are 60 and 50 mm wide. Plasma is produced when the upper parallel electrode (inlet) is driven by the HF sinusoidal voltage: $V = V_{\rm HF}\sin(2\pi f_{\rm HF}t)$; the lower parallel electrode (wafer), is driven by the LF sinusoidal voltage: $V = V_{\rm LF}\sin(2\pi f_{\rm LF}t)$. The LF is not necessary for generating the plasma, yet when added, it can control the velocity distribution of ions incident on the wafer[13]. The walls of the chamber are grounded. Two capacitors are connected to the wafer and the inlet separately, both with a capacitance of 1×10^{-7} F/m^2, and self-bias is calculated in the model. The coordinate system is illustrated in Fig. 2, with the direction of the x axis downwards and y axis outwards in the positive direction. A high-density plasma is generated when the gas flows in the inlet discharges are powered by the RF sources, and the remaining gas is pumped out through the outlet by the molecular pump. N_2 is taken as the discharge gas. The fixed inlet mass flow rate is 8000 sccm and the outlet flow is adapted by the inlet gas flow to keep the pressure steady in the chamber. The wall temperature is kept at 300 K, and about 3500 grids are generated.

Five problem types are included in this simulation: flow, chemistry, plasma, electric and magnetic field. We use the CCP's transient mode to solve them and the HF period is divided by 40 time steps. The initial conditions are set as follows: 300 K, 2 eV, 8000 sccm, 2.2 Torr. The gas composition is the same as in the inlet, outlet and initial conditions, as shown in Table 1. The volume and surface reactions are shown in Table 2. The reaction rate coefficients can be calculated from the collision cross-section[14] or the Arrhenius step type expressed as $k = \mathrm{ApTenexp}(-E_a/RT_e)$. For the collision cross-section, the minimum excitation energy is given in Table 2, where V means vibrational level. Secondary electrons are not considered.

Table 1. Correspondence value of MCy and yield.

x	Mass fraction
N_2	0.99999
N_2^+	0.000005
N	0.000005

The number density for electrons, ions and neutrals can be solved using the continuity and momentum equations[15], which are expressed as

$$\frac{\partial n}{\partial t} + \nabla\cdot\boldsymbol{\Gamma} = S, \tag{1}$$

$$\frac{\partial(m\boldsymbol{\Gamma})}{\partial t} + \nabla\cdot(m\boldsymbol{\Gamma}\boldsymbol{u}) = qnE - \nabla p - m\boldsymbol{\Gamma}\boldsymbol{\nu}_{\rm m}. \tag{2}$$

The variables n, m, q, p, $\boldsymbol{u}$ and $\boldsymbol{\nu}_{\rm m}$ stand for the density, mass, charge, pressure, velocity and collision frequency of each particle, respectively. S is the source of particles generated or consumed in chemical reactions, and E stands for the electric field intensity vector. For an ideal gas, pressure can be expressed in the form $p = nk_{\rm B}T$, where n is the particle density, $k_{\rm B}$ is the Boltzmann constant and T is the gas temperature. A Maxwellian velocity distribution is assumed since the pressure is not too low. Equation (2) can be simplified to the drift–diffusion approximation for electrons as:

$$\boldsymbol{\Gamma}_{\rm e} = n\boldsymbol{u} = \mu_{\rm e}n_{\rm e}\nabla\varphi - D_{\rm e}\nabla n_{\rm e},$$

where $\mu_{\rm e}$ is the electron mobility, the diffusion coefficient $D_{\rm e} = \frac{k_{\rm B}T_{\rm e}}{2m_{\rm e}\nu_{\rm e,n}}$, and they satisfy the Einstein relation. φ is the electrostatic potential, and $\nabla\varphi = -E$. Without considering reflection and secondary emission, the electron flux normal to the electrodes or walls is given by $\boldsymbol{\Gamma}_{\varepsilon,n} = \frac{1}{4}n_\varepsilon\nu_{\varepsilon,\rm th}$, where $\nu_{\varepsilon,\rm th} = \sqrt{8k_{\rm B}T_\varepsilon/\pi m_\varepsilon}$ is the electron thermal velocity.

The energy equations for electrons and heavy particles (ions and neutrals) are expressed as

$$\frac{3}{2}\frac{\partial}{\partial t}(n_{\rm e}T_{\rm e}) + \nabla\cdot\left(\frac{5}{2}T_{\rm e}\boldsymbol{\Gamma}_{\rm e} - \chi\nabla T_{\rm e}\right) = P - n_{\rm e}\sum_i n_i k_i \varepsilon_i, \tag{3}$$

Table 2. Reactions in N_2 plasma.

No		Reaction	Note
R1	Elastic collision	$N_2 \rightarrow N_2$	Elastic momentum transfer
R2	Excitation	$N_2 + E \rightarrow N_2 + E$	0.02 eV, N_2 rotational excitation
R3	Excitation	$N_2 + E \rightarrow N_2 + E$	0.29 eV, N_2 ($V = 1$)
R4	Excitation	$N_2 + E \rightarrow N_2 + E$	0.291 eV, N_2 ($V = 1$),
R5	Excitation	$N_2 + E \rightarrow N_2 + E$	0.59 eV, N_2 ($V = 2$)
R6	Excitation	$N_2 + E \rightarrow N_2 + E$	0.88 eV, N_2 ($V = 3$)
R7	Excitation	$N_2 + E \rightarrow N_2 + E$	1.17eV, N_2 ($V = 4$)
R8	Excitation	$N_2 + E \rightarrow N_2 + E$	1.47 eV, N_2 ($V = 5$)
R9	Excitation	$N_2 + E \rightarrow N_2 + E$	1.76 eV, N_2 ($V = 6$)
R10	Excitation	$N_2 + E \rightarrow N_2 + E$	2.06 eV, N_2 ($V = 7$)
R11	Excitation	$N_2 + E \rightarrow N_2 + E$	2.35 eV, N_2 ($V = 8$)
R12	Excitation	$N_2 \rightarrow N_2*$	6.17 eV, N_2 electronic (A3 $V = 0$–4)
R13	Excitation	$N_2 \rightarrow N_2*$	7 eV, N_2 electronic (A3 $V = 5$–9)
R14	Excitation	$N_2 \rightarrow N_2*$	7.35 eV, N_2 electronic (B3)
R15	Excitation	$N_2 \rightarrow N_2*$	7.36 eV, N_2 electronic (W3)
R16	Excitation	$N_2 \rightarrow N_2*$	7.8 eV, N_2 electronic (A3 $V = 10$–)
R17	Excitation	$N_2 \rightarrow N_2*$	8.16 eV, N_2 electronic (B'3)
R18	Excitation	$N_2 \rightarrow N_2*$	8.4 eV, N_2 electronic (a'1)
R19	Excitation	$N_2 \rightarrow N_2*$	8.55 eV, N_2 electronic (a1)
R20	Excitation	$N_2 \rightarrow N_2*$	8.89 eV, N_2 electronic (w1)
R21	Excitation	$N_2 \rightarrow N_2*$	11.03 eV, N_2 electronic (C3)
R22	Excitation	$N_2 \rightarrow N_2*$	11.87 eV, N_2 electronic (E3)
R23	Excitation	$N_2 \rightarrow N_2*$	12.25 eV, N_2 electronic (a"1)
R24	Excitation	$N_2 \rightarrow N_2*$	13 eV, N_2 sum of singlet states
R25	Ionization	$N_2 + E \rightarrow N_2^+ + 2E$	15.6 eV
R26	Dissociation	$N_2 + E \rightarrow 2N + E$	Ap $= 2.686 \times 10^{-14}$, $E_a/R = 13.421$
		Surface (S) mechanisms	Sticking coefficient
S1	Recombination	$N_2 + \rightarrow N_2$	Ap $= 1$, $E_a/R = 0$
S2	Recombination	$2N \rightarrow N_2$	Ap $= 0.005$, $E_a/R = 0$

$$\frac{\partial}{\partial t}(nC_pT) + \nabla \cdot (nC_pTu - k\nabla T) = - p(\nabla \cdot u) + \dot{Q} + n_e \sum_i n_i k_i \varepsilon_i, \quad (4)$$

where T_e is the electron temperature, n_e is the electron density, n is the number density of heavy particles, k is the thermal conductivity, and C_p is the specific heat at constant pressure. The energy transfer is due to convective flux and thermal diffusion, with coefficient $\chi = \frac{5}{2} n_e D_e$. The power density P stands for the energy absorbed by electrons, such as Joule heating P_{Joule}, inductive heating P_{ind} and external heating P_{ext}.

$$P = P_{Joule} + P_{ind} + P_{ext}, \quad (5)$$

where Joule heating[16] is $P_{Joule} = \boldsymbol{j}_e + \boldsymbol{E} = e\boldsymbol{\Gamma}_e \cdot \nabla\phi$; $\boldsymbol{E}$ is the induced electric field from time-varying magnetic field, and can be calculated in the electric and magnetic model: $\boldsymbol{E} = -\nabla\varphi - \frac{\partial \boldsymbol{A}}{\partial t}$, where φ and $\boldsymbol{A}$ are the electrostatic potential and magnetic vector potential respectively, and can be solved using Maxwell's equations with the finite volume method (FVM). There is no inductive heating here. External heating, that is stochastic heating, is not considered since the pressure is not low enough. $\sum_i n_i k_i \varepsilon_i$ stands for the energy loss from the collision between electrons and heavy particles, where n_i, k_i and ε_i are respectively the density, energy and coefficient of collision energy loss of the particle species[13]. $\dot{Q}$ represents the ion ohmic heating, which is given as

$$\dot{Q} = \sum\nolimits_{q_i} q_i n_i \mu_i \boldsymbol{E} \cdot \boldsymbol{E}, \quad (6)$$

where q_i, n_i, μ_i stand for the electric quantity, number density and mobility of ions, respectively. $\boldsymbol{E}$ is the electric field intensity.

3. Results and discussion

Figure 2 shows the 2D distribution of the electron number density under the condition $V_{HF} = 300$ V, $f_{HF} = 13.56$ Hz, $V_{LF} = 0$ V. N_e decreases gradually from the centre to the electrodes because the neutralization reaction occurs more quickly for the electrons and ions near the electrodes. N_e near the two ends of the electrode is larger than in the center, probably because of the long narrow space and high velocity which leave little time for the plasma in the middle to react efficiently.

In order to understand how the distributions of E_{pot} and N_e change in a cycle, we detect a 1D distribution of E_{pot} and N_e on different HF phases along the line $y = 90$ mm, as shown in Figs. 3 and 4, separately. Generally, most of the bulk space has the same E_{pot} at any time, while regulated by the transient RF voltage on the electrode as well as the E_{pot} in the sheath. N_e is modulated by E_{pot} in the sheath, from 0 to 3 mm near the upper electrode and from 11 to 14 mm near the lower electrode. The electrons come nearest to the upper electrode at the time when the phase of HF is $\pi/2$, because the HF bias voltage is positive and the potential drop between the upper electrode and the plasma bulk becomes small. When the phase of HF is $3\pi/2$, the

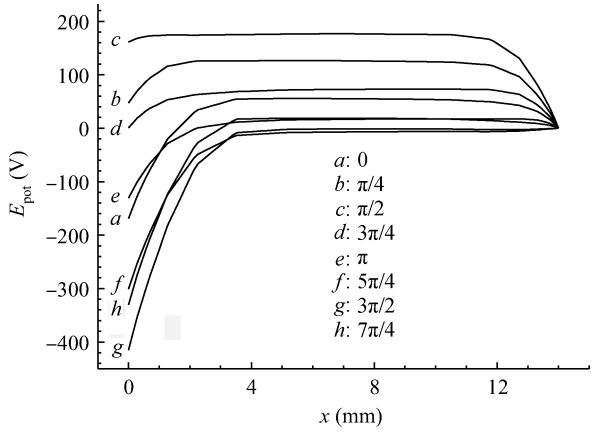

Fig. 3. Dependence on spatial distribution of E_{pot} on different HF phases ($y = 90$ mm).

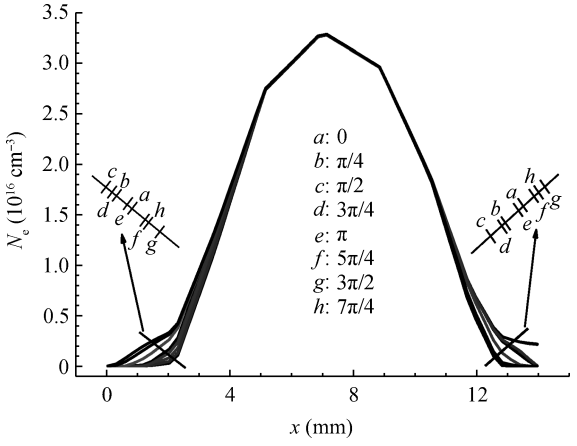

Fig. 4. Dependence on spatial distribution of Ne on different HF phases ($y = 90$ mm).

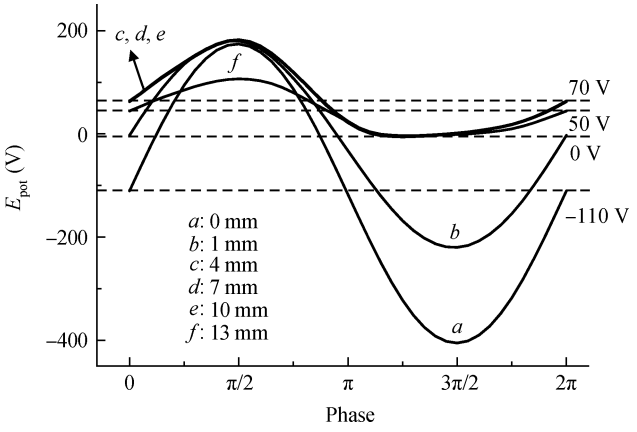

Fig. 5. Dependence on phase change of E_{pot}.

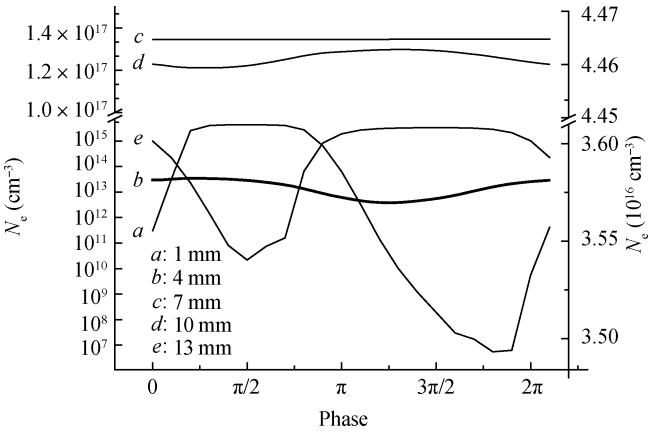

Fig. 6. Dependence on phase change of N_e ($y = 90$ mm).

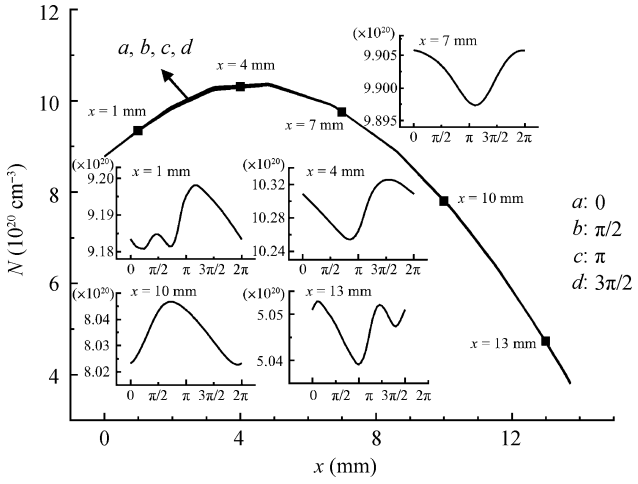

Fig. 7. Dependence on spatial distribution and phase change of N.

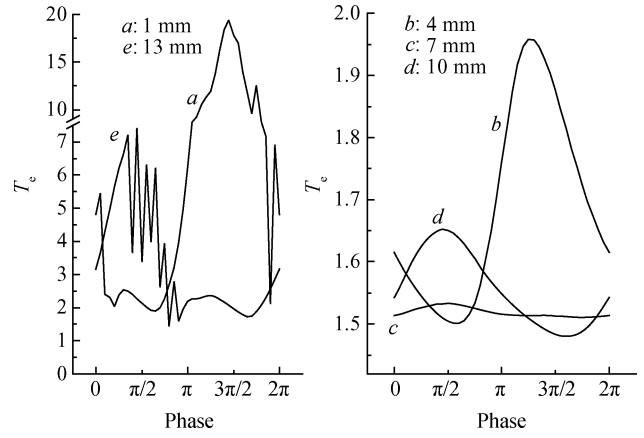

Fig. 8. Dependence on phase change of T_e.

large potential drop at the upper electrode repels the electrons, resulting in almost zero density of electrons in the sheath region. The results are in accordance with that of the simulation made by Wakayama and Nanbu[13], ignoring the small differences in the values of voltage, frequency and phase, however.

E_{pot} and N_e at 5 positions ($x = 1$, 4, 7, 10,13 mm) in the direction of $y = 90$ mm in a cycle are detected, as shown in Figs. 5 and 6, respectively. The nearer to the upper electrode, the larger the amplitude of E_{pot} at that point. There is a bias voltage of about –110 V on the surface of the upper electrode ($x = 0$ mm), and 70 V in the plasma bulk. In the plasma bulk from $x = 4$ mm to $x = 10$ mm, E_{pot} changes synchronously, keeping N_e almost the same in a cycle. As a result, we can estimate how some influential factors, such as the values of HF and LF voltages, affect electron number density by comparing

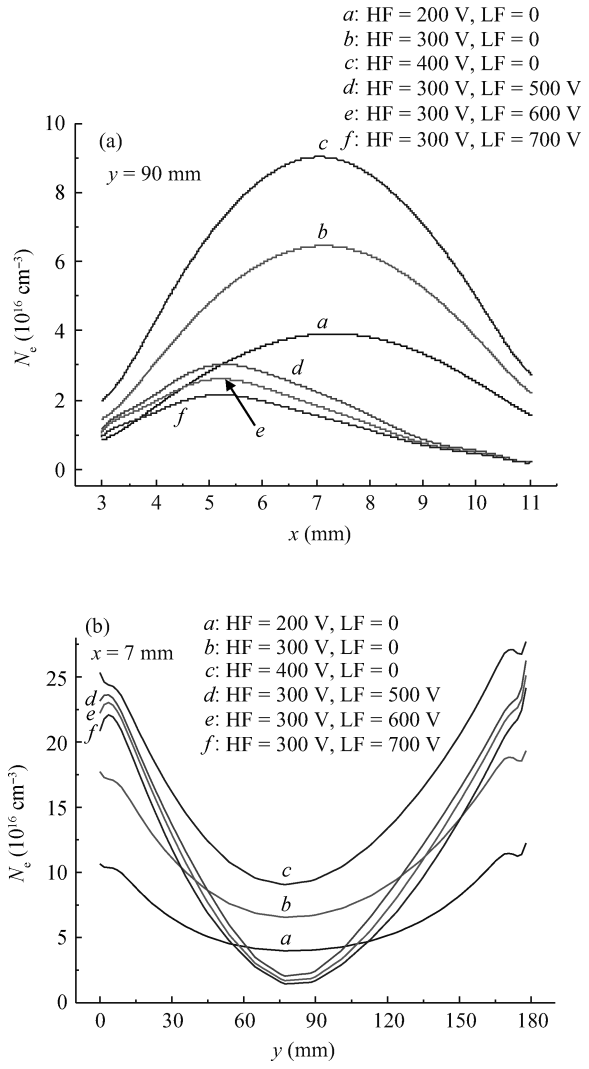

Fig. 9. The influence of voltages for HF = 13.56 MHz, LF = 0.3 MHz.

N_e in the plasma bulk.

Figures 7 and 8 show the distribution of N number density (N) and electron temperature (T_e), separately. N and T_e in the plasma bulk vary little during a cycle while Te in the sheath varies a lot. This is because the strong electron field in the sheath accelerates the electrons and result in high electron energy. Collisions with other particles during acceleration may cause the fluctuation in the sheath.

To understand the influence of HF voltage, we compared N_e from 3 to 11 mm at $y = 90$ mm in Fig. 9(a) and from 0 to 180 mm at $x = 7$ mm in Fig. 9(b), with LF = 0.3 MHz at 0 V, HF = 13.56 MHz at 200 V, 300 V, 400 V and HF = 13.56 MHz at 300 V, LF = 0.3 MHz at 500 V, 600 V, 700 V, separately. When the solver comes to a steady cycle, as shown in Fig. 9(a), N_e increases with the increase of the HF voltage because when the voltage increases, more N_2 are likely to be ionized and more energy will enter the plasma. When the LF voltage increases with fixed HF voltage, the ions' bombardment energy towards the wafer will increase as the self-bias voltage increases. But it will be less likely to meet the condition for generating high plasma density[17]: $\omega_H^2 |V_H| \gg \omega_L^2 |V_L|$, resulting in a decrease of N_e instead. However, the influence of LF voltage on N_e is not as obvious as that of HF voltage. Compared with single-frequency (LF = 0 V), N_e decreases in both the $y = 90$ mm and $x = 7$ mm directions, while the homogeneity of N_e increases in the direction of $y = 90$ mm and decreases in the direction of $x = 7$ mm.

4. Conclusion

Using the CFD-ACE+ software package, the governing equations of the CCP option, which solves the most general equation set of the plasma fluid model, are applied to both plasma and sheath regions. The electron transport equation and electron energy equation are solved for the electron number density, and the electrostatic field is obtained by solution of the Poisson equation. This paper illustrates the distribution of E_{pot}, N_e, N and Te under the conditions HF = 13.56 MHz at 300 V, LF = 0.3 MHz at 0 V, and the influence of HF and LF on N_e are discussed under the conditions of different HF voltages of 200 V, 300 V, 400 V with HF = 13.56 MHz, LF = 0 V, and different LF voltages of 500 V, 600 V, 700 V with LF = 0.3 MHz, HF = 13.56 MHz @ 300 V, separately.

The results show that the distribution of N_e is like a saddle surface, where the center of N_e is highest in the x direction and lowest in the y direction. The sheaths near the two electrodes are about 3 mm, within which E_{pot} varies and is regulated by the varying electrode voltage. In the plasma bulk from $x = 4$ mm to $x = 10$ mm, E_{pot} changes synchronously with the largest bias voltage of about 70 V, keeping E_{pot} in the bulk positive at all times. N_e, which is decided by the distribution of E_{pot}, varies extensively in the sheath and stays almost the same in the bulk where there is no electric potential difference. Through comparing the N_e in the bulk under different HF and LF voltages, we know that lower HF voltage and higher LF voltage in dual-frequency will decrease N_e while the homogeneity of N_e changes differently between the x and y directions. In addition, decreasing the LF voltage is not as efficient as increasing the HF voltage, and it will reduce the energy of impinging ions in the electrode sheath. As a result, appropriate HF and LF voltages need to be chosen carefully in order to obtain a balance between high-density and homogeneous plasma.

Much more research and simulations remain to be carried out concerning the characteristics of plasma parameters under different conditions of HF and LF. I will continue my research on the influence of different frequencies, with one frequency as 13.56 MHz and another from 0.3 to 60 MHz, for example. All of these can be viewed as reference for the development of dual-frequency PECVD devices.

References

[1] Rakhimova T V, Braginsky O V, Ivanov V V, et al. Experimental and theoretical study of ion energy distribution function in single and dual frequency RF discharges. IEEE Trans Plasma Science, 2007, 35(5): 1229

[2] Zhu X M, Pu Y K. A simple collisional-radiative model for low-pressure argon–oxygen mixture discharges. J Phys D: Appl Phys, 2007, 40: 5202

[3] Zhu X M, Pu Y K. Using OES to determine electron temperature and density in low-pressure nitrogen and argon plasmas. Plasma Sources Sci Technol, 2008, 17: 024002

[4] Zhu X M, Chen W C, Li J, et al. Determining the electron tem-

perature and the electron density by a simple collisional-radiative model of argon and xenon in low-pressure discharges. J Phys D: Appl Phys, 2009, 42: 025203

[5] Georgieva V, Bogaerts A. Numerical simulation of dual frequency etching reactors: influence of the external process parameters on the plasma characteristics. J Appl Phys, 2005, 98: 023308

[6] Salabas A, Brinklmann R P. Numerical investigation of dual frequency capacitively coupled hydrogen plasmas. Plasma Sources Science and Technology, 2005, 14: S53

[7] Dai Z L, Xu X, Wang Y N. A self-consistent hybrid model of a dual frequency sheath: Ion energy and angular distributions. Phys Plasmas, 2007, 14: 013507

[8] Wang S, Xu X, Wang Y N. Numerical investigation of ion energy distribution and ion angle distribution in a dual-frequency capacitively coupled plasma with a hybrid model. Phys Plasmas, 2007, 14: 113501

[9] Guan Z Q, Dai Z L, Wang Y N. Simulations of dual rf-biased sheaths and ion energy distributions arriving at a dual rf-biased electrode. Phys Plasmas, 2005, 12: 123502

[10] Wang Shuai. The hybrid simulation of a dual-frequency capacitively coupled plasma. PhD Dissertation, Dalian: Dalian University of Technology, 2008 (in Chinese)

[11] Ventzek P L G, Hoekstra R J, Kushner M J. Two-dimensional modeling of high plasma density inductively coupled sources for materials processing. J Vac Sci Technol B, 1994, 12(1): 461

[12] Rakhimova T V, Braginsky O V, Ivanov V V, et al. Experimental and theoretical study of RF plasma at low and high frequency. Special Issue of the IEEE Transactions on Plasma Science, Eindhoven, The Netherlands, 2006, 34(3): 867

[13] Wakayama G, Nanbu K. Velocity distribution of ions incident on a wafer in two frequency capacitively-coupled plasmas. Institute of Fluid Science, Tohoku University, Katahira 2-1-1, Aoba-ku, Sendai, Japan 980-8577

[14] Phelps A V, Pitchford L C. Anisotropic scattering of electrons by N_2 and its effect on electron transport. Phys Rev A, 1985, 31: 2932

[15] CFD-ACE+. 2009, CFD-ACE+ WebHelp, ESI-Group, Paris, France

[16] Kolobov V I, Economou D J. The anomalous skin effect in gas discharge plasmas. Plasma Sources Sci Technol, 1997, 6: R1

[17] Lieberman M A, Lichtenberg A J. Principles of plasma discharge and materials processing. 2nd ed. New Jersey: John Wiley and Sons Inc, 2005